

UCSF

UC San Francisco Previously Published Works

Title

Abdominal and pelvic imaging findings associated with sex hormone abnormalities.

Permalink

<https://escholarship.org/uc/item/7cq623wg>

Journal

Abdominal radiology (New York), 44(3)

ISSN

2366-004X

Authors

Kurzbard-Roach, Nicole
Jha, Priyanka
Poder, Liina
[et al.](#)

Publication Date

2019-03-01


DOI

10.1007/s00261-018-1844-1

Peer reviewed



Abdominal and pelvic imaging findings associated with sex hormone abnormalities

Nicole Kurzbard-Roach¹ · Priyanka Jha¹  · Liina Poder¹ · Christine Menias²

© Springer Science+Business Media, LLC, part of Springer Nature 2018

Abstract

Hormones are substances that serve as chemical communication between cells. They are unique biological molecules that affect multiple organ systems and play a key role in maintaining homeostasis. In this role, they are usually produced from a single organ and have defined target organs. However, hormones can affect non-target organs as well. As such, biochemical and hormonal abnormalities can be associated with anatomic changes in multiple target as well as non-target organs. Hormone-related changes may take the form of an organ parenchymal abnormality, benign neoplasm, or even malignancy. Given the multifocal action of hormones, the observed imaging findings may be remote from the site of production, and may actually be multi-organ in nature. Anatomic findings related to hormone level abnormalities and/or laboratory biomarker changes may be identified with imaging. The purpose of this image-rich review is to sensitize radiologists to imaging findings in the abdomen and pelvis that may occur in the context of hormone abnormalities, focusing primarily on sex hormones and their influence on these organs.

Keywords Hormone · Reproductive endocrinology · Estrogen · Ultrasound · MRI

Introduction

Hormones are chemical substances that participate in communication between cells [1]. Hormonal abnormalities may occur in the setting of abnormal function of an endocrine gland, abnormal production or conversion by a neoplasm, or increased conversion of precursor molecules. Hormones are synthesized throughout the body and have different mechanisms of action in different tissues, and are uniquely biologically active, potentially acting on multiple organ systems simultaneously.

Hormone levels may be either abnormally increased or decreased. If imaging findings are present, this is usually in the context of increased hormone levels (overproduction or decreased breakdown). A hormone may have an effect on a tissue even if that structure is not a “target organ” of the

hormone. Sex hormones are an important part of the human internal milieu and have multiple target and non-target sites upon which they act. For example, the target organs of estrogen are the breasts, uterus, ovaries, bone marrow, and brain, but circulating estrogens and metabolites additionally affect liver, skin, and other organs [2, 3]. As such, while elevated estrogen levels are intuitively expected to affect the reproductive tract, imaging findings may also be seen throughout the abdomen and pelvis, including in the liver and skeletal system. Certain imaging findings in the abdomen and pelvis may be the direct or indirect result of hormone abnormalities. This review, organized by organ system, addresses common sex hormone-related abnormalities that may be identified at imaging of the abdomen and pelvis. A summary of findings organized by organ system is presented in Table 1.

Estrogen

Estrogen is the primary hormone involved in the development and function of the female reproductive system. Estrogen is mainly produced by the ovaries in pre-menopausal women and from fat in post-menopausal women [2].

✉ Priyanka Jha
Priyanka.Jha@ucsf.edu

¹ Department of Radiology and Biomedical Imaging,
University of California, San Francisco, San Francisco, CA,
USA

² Department of Radiology, Mayo Clinic, Scottsdale, AZ, USA

Table 1 Imaging findings

	Imaging features
Hepatobiliary	
Focal nodular hyperplasia	US: solid lesion, variable echogenicity relative to liver CT and MRI: arterially hyperenhancing, delayed enhancement of central scar with extracellular contrast, retention of hepatobiliary contrast agents at hepatobiliary phase MRI
Hepatocellular adenoma	See Table 2
Budd–Chiari syndrome	US: thrombus, altered flow in hepatic veins; enlarged caudate lobe; ascites; splenomegaly CT/MRI: hepatic vein thrombus; regenerative nodules; enlarged caudate lobe; ascites; splenomegaly Angiography: “spiderweb” intrahepatic collateral vessels; compression of IVC by enlarged caudate lobe
Reproductive	
Endometrial hyperplasia	US: endometrial thickening and/or cystic change MRI: endometrial thickening and/or cystic change
Endometrial carcinoma	US: endometrial thickening and/or focal mass; possible increased vascularity MRI: endometrial thickening and/or focal mass
Clear cell adenocarcinoma of the vagina or cervix	US: vaginal and/or cervical solid mass MRI: vaginal and/or cervical solid, enhancing mass
Polycystic ovarian syndrome	US and MRI: > 26 small, peripheral ovarian follicles without dominant follicle
Theca lutein cysts	US and MRI: enlarged ovaries with multiple enlarged follicles May see causative etiology for elevated HCG, including gestational trophoblastic disease.
Ovarian hyperstimulation syndrome	US, CT, MRI: enlarged ovaries with multiple enlarged, heterogeneous follicles; pelvic free fluid
Endometrioma	US: cystic ovarian lesion with diffuse low-level echoes, mural echogenic foci MRI: cystic ovarian lesion which is T1 hyperintense, T2 intermediate with “shading” and possible T2 hypointense “dark spot”
Sex cord-stromal tumors	US and MRI: heterogeneous ovarian mass, can be multicystic with intracystic hemorrhage

Cell lines within fat tissue, from mesenchymal stem cells to mature cell types, are a major site of activity of aromatase (estrogen synthetase), the enzyme responsible for converting circulating androgens to estrogens [4]. As visceral fat is relatively increased in obese patients, circulating estrogens are increased in these patients as well [4].

Hepatobiliary

The liver is one of the most hormonally active organs in the abdomen, playing a crucial role in cholesterol metabolism. It is involved in both the production and the processing of estrogen. Hepatocytes function as a site of estrogen synthesis via aromatase (estrogen synthase), as well as serve to biotransform estradiols to various metabolites [2, 5]. In turn, estrogen and its metabolites act directly on hepatocytes, stimulating growth and influencing metabolism [2]. Hepatobiliary findings in the setting of excess estrogen range from steatosis to neoplasm to vascular thrombosis.

Focal nodular hyperplasia

Focal nodular hyperplasia (FNH) is the most common benign hepatic neoplasm, with the prevalence reported between 0.2% in an imaging series of over 45,000 patients and 3% in a necropsy series of 95 patients [6–8]. Marked female predominance, with female:male ratio reported to range from 2:1 to 26:1, supports the theory that estrogen exposure may play a role in its development, including exogenous exposure from oral contraceptive pills (OCPs) or hormone replacement therapy (HRT). Histologically, FNH is composed of hyperplastic proliferation of benign hepatocytes, ducts, and vessels, however, lacks normal portal triad architecture [6]. Most patients with FNH are asymptomatic and FNH are mostly incidentally detected. Symptoms of vague abdominal pain or discomfort may arise when an FNH is large (> 5 cm) or subcapsular in location [9, 10]. In 70% of cases, FNH is a solitary lesion, with multiple lesions seen in remainder of the cases [10]. Rarely, FNH can rupture and present with hemoperitoneum, though hemorrhage is more common with other neoplasms, specifically hepatic adenomas [11].

Table 2 Hepatocellular adenoma

Subtype	Mutation/genotypic expression	% of adenomas	Hormonal risk factors	Imaging features	Malignant potential
Steatotic	HNF1a (Hepatic nuclear factor 1-alpha) inactivation Lack expression of liver-fatty acid binding protein (L-FABP)	35–50	Oral contraceptives	Signal loss on opposed-phase MRI imaging	Rare
Beta-catenin mutated	CTNNB1 (Beta-catenin) activation	10–15	Anabolic steroids	No specific features. May have vague central scar. May take up hepatobiliary contrast agent.	High
Inflammatory	SAA (serum amylase A) and CRP (C-reactive protein) expression	25–35	Oral contraceptives	“Atoll” sign of peripheral and central T2 hyperintense signal	Up to 10% if beta-catenin mutation also present; otherwise low
Unclassified		5–10		No specific features	

At ultrasound (US), FNH is a non-specific solid lesion with variable echogenicity, and may appear hyperechoic or hypoechoic relative to adjacent liver parenchyma, particularly as there is considerable patient-to-patient variability in background hepatic parenchymal echogenicity [12, 13]. A hypoechoic central stellate scar may be present. With color Doppler sonography, a spoke-wheel pattern may sometimes be present with vascularity radiating peripherally from the central nidus (Fig. 1). Contrast-enhanced multiphase CT or MRI can be diagnostic for FNH. With CT, the classic imaging appearance of the lesion is arterial phase hyperenhancement with central stellate non-enhancement. This non-enhancing area corresponds to a central bundle/nidus of fibrous and vascular tissue, or “central scar” [14]. On delayed phase, the mass is isodense to the liver with delayed central scar hyperenhancement. On venous phase, FNH is usually isodense to the background liver, and often not visualized, earning the

descriptor “stealth” tumor [15]. With multiphase MRI, the lesion appears hyperintense on T2-weighted images and iso- to hypointense on T1-weighted images (Fig. 2). With contrast enhancement, there is similar arterial phase hyperenhancement without arterial phase enhancement of the central scar. FNH then becomes isointense to the background liver on the venous and equilibrium phase. The appearance of FNH on delayed phase MRI varies depending on the excretory patterns of the contrast agent used (Fig. 2). Specifically, the central scar will demonstrate delayed enhancement with extracellular contrast, while the lesion parenchyma will become isointense to the liver [12]. With hepatobiliary contrast agents, the lesion will demonstrate hepatobiliary hyperintensity as the benign proliferation of hepatocytes constituting the lesion demonstrate uptake of the hepatobiliary contrast but excretion is altered due to disorganized biliary architecture within the lesion (Fig. 2) [12].

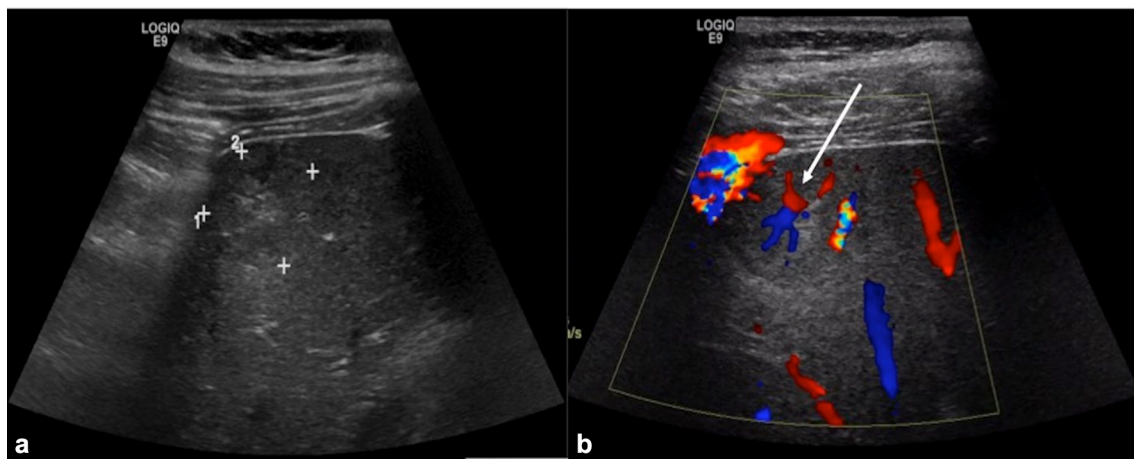


Fig. 1 A 31-year-old woman with elevated liver enzymes in the setting of oral contraceptive use. **a** Grayscale ultrasound image demonstrates a subtle isoechoic lesion (calipers) with hyperechoic

center. **b** On Color Doppler imaging, “spoke-wheel” vascularity emanating from a central nidus is seen (arrow), suggestive of focal nodular hyperplasia

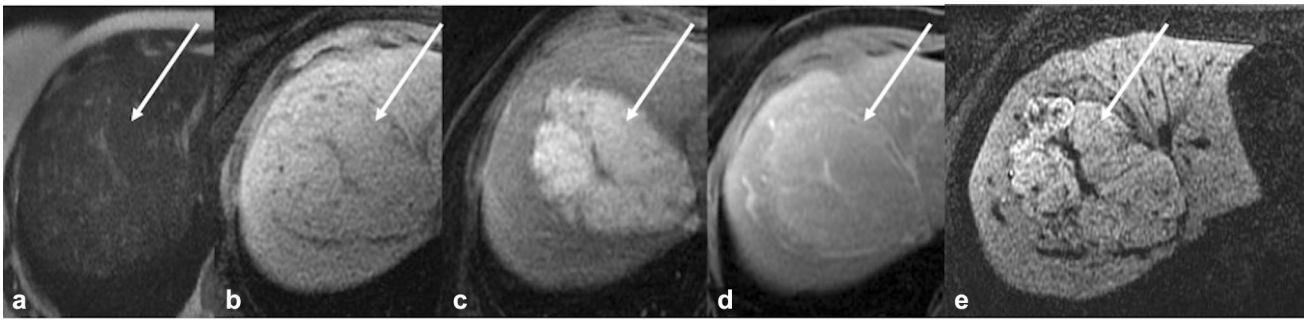


Fig. 2 A 35-year-old woman who presented with abdominal pain. History of > 10 years oral contraceptive use. **a** Axial T2-weighted, **b** T1-weighted, **c** arterial phase, **d** venous phase, and **e** hepatobiliary phase MR images show subtly T2 hyperintense, T1-isointense,

arterially enhancing mass with non-enhancing central “scar” and retention of contrast on hepatobiliary phase, most consistent with focal nodular hyperplasia

FNH is usually considered a benign lesion; however, it can continue to grow, particularly if the inciting cause is not altered. Specifically, enlargement has been reported with pregnancy and continued OCP use [11]. Malignant transformation to HCC is considered an extremely rare scenario, and to date, only 22 cases of pathologically proven malignant degeneration of FNHs have been reported [16]. For asymptomatic lesions less than 4 cm in size, imaging surveillance and conservative management is probably appropriate [9, 16]. A definitive imaging surveillance interval has not been reported in the literature but larger lesions can be followed at 6-month intervals [11]. When lesions grow or become symptomatic, in addition to removing aggravating factors, other treatment options such as surgical resection, radiofrequency ablation, and transarterial chemoembolization may be appropriate based on a center’s expertise and preference [16]. However, there is lack of evidence-based literature to support the use of one strategy over the other and continued research is expected in this field [11]. Lesions have been reported to spontaneously regress, both in the clinical setting of cessation of hormone use as well as independent of changes in exogenous hormone exposure [17]. More investigation into the natural history of these lesions may reveal a stronger association of FNH regression with cessation of OCPs or HRT.

Hepatocellular adenoma

Hepatocellular adenomas are, as a group, the second most common benign hepatic neoplasm [6]. The major risk factor for development is exposure to steroid hormones, such as anabolic steroids and OCPs [5]. Women over 30 years of age with more than 5 years of OCP use have the highest risk levels [11]. Unlike FNH, adenomas are associated with abdominal pain, which has been posited to occur in the setting of intralesional hemorrhage and necrosis [13]. Patients may also have abnormal alkaline

phosphatase (ALK-P) and/or gamma-glutamyl transferase (GGT) levels in the setting of very large lesions [18]. Adenomas are categorized into subtypes depending on the associated mutation and genotypic expression, and are summarized in Table 2. Hepatocyte nuclear factor 1-alpha (HNF1a) subtype lesions, also described as steatotic, and inflammatory subtype lesions occur primarily in the presence of estrogen exposure, specifically oral contraceptives. Beta-catenin-activated subtype adenomas occur primarily in the setting of androgenic steroid exposure, typically exogenous; this is the most common subtype identified in men with hepatocellular adenomas [18]. While adenomas are benign lesions, the risk of intralesional or perilesional hemorrhage increases when an adenoma grows larger than 5 cm in size [9, 10]. Additionally, malignant transformation to hepatocellular carcinoma (HCC) has been reported with beta-catenin subtype lesions, particularly in men [18, 19].

Adenoma appearance can vary at ultrasound, presenting as hyperechoic or hypoechoic lesions (Fig. 3). CT demonstrates these lesions to be arterially hyperenhancing with occasional washout (Fig. 4) [13]. Imaging features of the different subtypes of hepatocellular adenoma can be best differentiated with MRI [13, 20, 21]. HNF1a-inactivated (steatotic) adenomas (35–50% adenomas) characteristically demonstrate intralesional fat, which is best appreciated as signal loss on opposed-phase gradient echo chemical shift sequences (Fig. 5). No specific imaging signature has been ascribed to the beta-catenin-activated subtype (10–15% adenomas); these lesions may demonstrate any number of features, including varying degrees of enhancement at multiphase imaging, excretion of hepatobiliary contrast agents, and/or presence of a central fibrous scar. Recent studies have confirmed that this lesion can be virtually indistinguishable from FNH and can show hepatobiliary hyperintensity; so appropriate clinical context can sometimes aid in distinction [22, 23]. This hepatobiliary hyperintensity correlates with the organic anion transporting polypeptide (OATP) level in benign hepatocellular

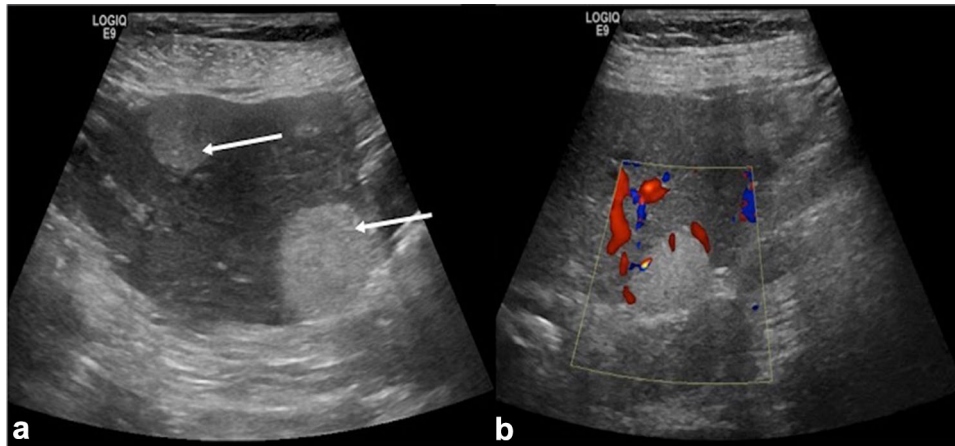


Fig. 3 A 48-year-old woman taking oral contraceptives. **a** Grayscale ultrasound image demonstrates two hyperechoic liver lesions, both biopsy-proven hepatocellular adenomas. **b** Color Doppler image shows no internal flow within one of the lesions. The imaging

appearance of these lesions is non-specific and overlaps with both benign and malignant etiologies. Contrast-enhanced CT or MR imaging is necessary for further characterization in the absence of tissue sampling

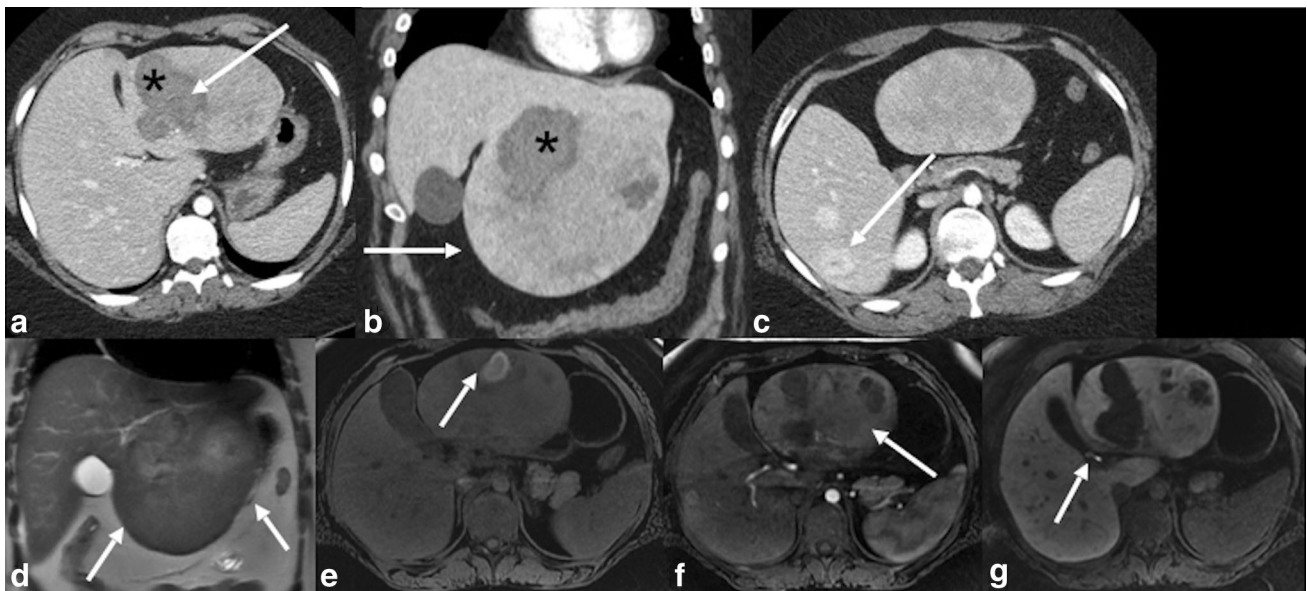


Fig. 4 A 21-year-old woman with history of OCP use who presented with acute abdominal pain. **a** Axial and **b** Coronal CT images demonstrate a large, exophytic heterogeneous hepatic mass (arrows). The mass is isoenhancing to the liver, suggestive of an adenoma, given the risk factors. Areas of non-enhancement (asterisk) are suspicious for hemorrhage. **c** Additional numerous hyperenhancing masses (arrows) were present, raising suspicion for adenomatosis. MR imaging was recommended for follow-up. Follow-up MR imaging was performed. **d** Coronal T2-weighted image demonstrates a heterogeneous exophytic mass (arrows). **e** T1-weighted image

demonstrates intrinsic T1 hyperintensity (arrow) suggestive of hemorrhage. **f** Post-contrast T1-weighted image in the arterial phase shows heterogeneous hyperenhancement of the mass. **g** Post-contrast T1-weighted image in the hepatobiliary phase demonstrates persistent hyperintensity of the lesion, a finding that can be seen in the presence of a beta-catenin activating mutation. Arrow demonstrates biliary excretion of hepatobiliary contrast agent. At tissue sampling, pathology revealed inflammatory adenoma with beta-catenin activation

tumors and may be explained by activation of the Wnt β -catenin pathway [22]. With inflammatory subtype lesions (25–35% adenomas), an “atoll” sign with T2-weighted MRI sequences has been described, denoting hyperintense T2 signal about the periphery and centrally within the lesion. Rarely, inflammatory adenomas too can mimic

FNH in imaging appearance, including hepatobiliary phase hyperintensity [23]. In these circumstances, conventional pathology may also be limited and true etiology of the mass is best ascertained with glutamine synthetase immunohistochemistry [24]. Unclassified adenomas (5–10%

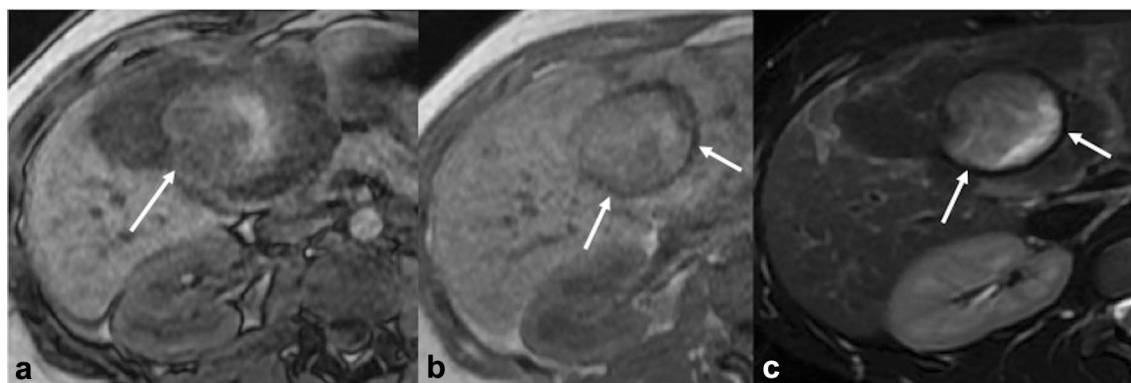


Fig. 5 A 32-year-old pregnant woman with acute right upper quadrant pain. **a** Axial opposed-phase gradient echo, **b** in-phase gradient echo, and **c** T2-weighted MR images show a large hepatic mass with lobulated contour. **a** The mass has diffuse signal loss on opposed-phase sequence (arrow), confirming the presence of

adenomas) do not have any specific genotypic, pathologic, nor imaging features [12, 20, 21].

Management of hepatocellular adenoma depends on subtype, size of lesion, and patient demographics. For women with lesion size less than 4–5 cm, who are taking OCPs or HRT, usual treatment includes cessation of hormones and annual imaging surveillance with contrast-enhanced CT or MRI [11]. With lesions > 5 cm, one particular management strategy proposed is for OCPs to be stopped and MRI performed after 6 months [11]. If the lesion has decreased to < 5 cm, definitive imaging signs to confirm that the lesion is a steatotic adenoma should be assessed. If steatotic adenoma is confirmed at imaging, management can potentially be less aggressive because the risk of malignant progression is very low. Follow-up should still be performed, initially every 6 months, and if the lesion shows no further alteration, follow-up can be stopped or repeated yearly until menopause [11].

For pregnant women, given the increased levels of circulating reproductive hormones, closer sonographic surveillance (every 3 months) is warranted due to risk of lesion growth [18, 25]. For women with lesions greater than 4–5 cm in size, percutaneous ablation or surgical consultation is generally recommended due to increased risk of hemorrhage (intralesional or lesion rupture) with increased lesion size (Fig. 5). Treatment of adenoma during pregnancy may be indicated if the lesion shows signs of growth or bleeding. Additional risk factors for hemorrhage include inflammatory subtype, lesion growth, and recent hormone use (within prior 6 months) [18]. First-line treatment of acute hemorrhage in a hemodynamically stable patient is transarterial embolization, while unstable patients may require immediate surgical intervention. For men, surgical excision is generally recommended rather than surveillance, given the elevated risk of

intralesional fat characteristic of a steatotic-type HNF1 α -inactivated hepatic adenoma. **b** Recurrent intralesional hemorrhage is demonstrated by peripheral hypointense signal on in-phase and **c** T2-weighted sequences (arrows). Heterogeneous signal intensity within the lesion is suggestive of large amount of intralesional hemorrhage

malignant transformation in male patients. Molecular evidence points to the small but definitive risk of malignancy with the beta-catenin-activated and inflammatory adenoma subtypes, particularly when the size is > 5 cm [11]. Hence, in this scenario, invasive surgical management is recommended [26]. While biopsy can be performed to confirm the diagnosis of beta-catenin mutated adenomas, surgical management remains the mainstay, especially with male sex, steroid use, glycogen storage disease, or underlying viral hepatitis [11].

Budd–Chiari syndrome

Estrogen increases blood coagulability by increasing both fibrinogen levels as well as the activity of clotting factors VII and X, and decreasing the activity of coagulation inhibitor antithrombin III [27, 28]. In the liver, hyperestrogenemic procoagulant states such as pregnancy or OCP use may result in hepatic vein thrombosis and Budd–Chiari syndrome [27, 29, 30]. Up to 47% of reported Budd–Chiari syndrome cases were encountered in women presenting in pregnancy or postpartum [31]. Risk of venous thrombus is particularly elevated in women with additional prothrombotic conditions such as protein C or S deficiency or Factor V Leiden mutation [29]. Additional major risk factors for hepatic vein thrombosis include other risks for hypercoagulability, including malignancy, bone marrow transplant, and liver transplant [30].

Budd–Chiari syndrome describes the constellation of clinical findings in the setting of hepatic venous outflow obstruction [32]. Obstruction may occur at any level within the hepatic venous system, from the venules to the suprahepatic inferior vena cava (IVC). The syndrome may be classified as one of three types depending on the level of obstruction: type I describes IVC occlusion with or without

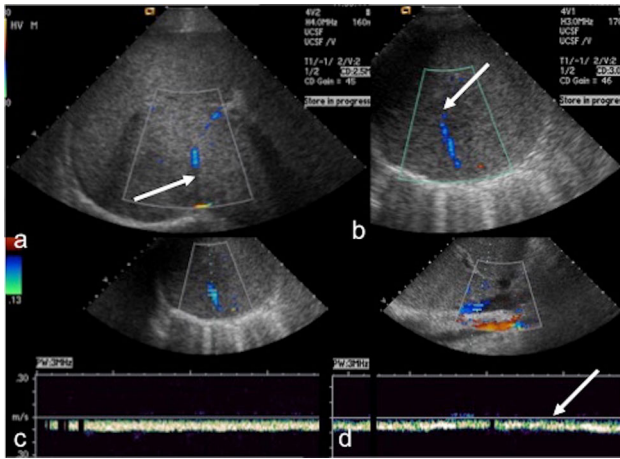


Fig. 6 A 33-year-old postpartum woman who presented with new ascites. **a, b** Doppler US images of the liver demonstrate interrupted flow between the middle and right hepatic veins. **c, d** Spectral Doppler interrogation of the right hepatic vein and IVC demonstrates abnormally monophasic waveforms and absent respiratory variation

involvement of the hepatic veins. Type II describes Budd–Chiari when the predominant occlusion involves the major hepatic veins; the IVC may or may not be involved to a lesser extent. Type III describes veno-occlusive disease, with occlusion primarily involving small centrilobular veins [33]. Clinical presentation includes abdominal pain and features of hepatic congestion, including hepatomegaly, splenomegaly, and ascites. In chronic untreated cases, cirrhosis and portal hypertension may develop, with resultant complications including varices and variceal bleeding [33].

Imaging manifestations of Budd–Chiari syndrome are varied and depend on the acuity of presentation and the

type/level of obstruction. At ultrasound, the most common findings are caudate lobe enlargement, ascites, and splenomegaly [32, 33]. Abnormally diminished or absent hepatic venous flow may be seen with Doppler ultrasound interrogation. Due to disrupted communication between the hepatic veins and IVC and the right atrium, the respiratory variability of the hepatic venous waveforms is lost and the waveforms become more monophasic (Fig. 6). In severe cases, reversal of flow in the hepatic veins and/or portal veins may also be seen [32]. Findings at contrast-enhanced CT are the same as at gray scale ultrasound, with the addition of heterogeneous attenuation of hepatic parenchyma, hypoenhancement of the involved thrombosed veins, and enhancement of prominent intrahepatic collateral vessels (Fig. 7) [33]. Chronic changes include calcification of thrombosed veins as well as development of regenerative nodules within the hepatic parenchyma. Although regenerative nodules enhance avidly at the arterial phase of post-contrast imaging, they retain contrast at the portal venous phase rather than washing out, enabling differentiation from HCC [34, 35]. Additionally, portal vein thrombosis may develop in the setting of severe venous outflow obstruction causing slow or stagnant flow in the portal system [33].

MRI and MR angiography are useful in evaluation of the liver parenchyma and vessel patency. In the acute setting, the hepatic parenchyma appears heterogeneous on T2-weighted and T1-weighted sequences, with differential prominent enhancement of the caudate lobe as compared to the remainder of the liver. Lack of enhancement of the thrombosed hepatic veins may be seen on post-contrast sequences. Regenerative nodules typically appear

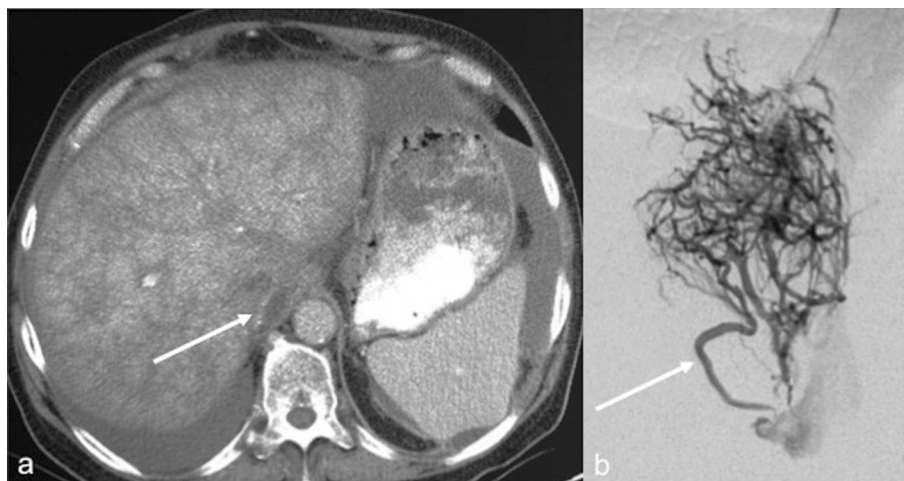


Fig. 7 A 17-year-old female smoker who presented with abdominal fullness after beginning oral contraceptives. **a** Axial contrast-enhanced CT at the level of the upper abdomen shows markedly heterogeneous enhancement of the hepatic parenchyma and only trace enhancement within the inferior vena cava (arrow). No flow was seen

in the hepatic veins (not shown). **b** Digital subtraction angiography (DSA) image in the AP projection obtained during inferior vena cavography shows the characteristic “spiderweb” appearance of collateral hepatic venous flow without discernible anatomic hepatic veins. Prominence of the caudate vein is also seen (arrow)

hypointense to surrounding parenchyma on T2-weighted sequences and hyperintense on T1-weighted sequences, enabling differentiation from HCC [34, 35]. With conventional angiography, the classic appearance of “spider-web” pattern of intrahepatic collateral vessels is seen following contrast administration within the inferior vena cava and/or hepatic veins (Fig. 7). Filling defects within the IVC and hepatic veins compatible with thrombus can also be seen. Additionally, narrowing of the IVC may be appreciated secondary to compression by the enlarged caudate lobe [32].

Treatment depends on the type/level of occlusion [36]. Patients with vessel thrombus are usually treated with anticoagulation. In high-risk pregnancies, low molecular weight heparins can be prescribed in the absence of contraindications. Type I occlusions are typically treated with IVC stenting, while types II and III may be treated with transjugular intrahepatic portosystemic shunt (TIPS) placement [33]. In the pregnant patient with Budd–Chiari syndrome, the prognosis is poor both for the mother and fetus even with treatment, with reports of spontaneous abortions, stillbirth, and preterm labor [29].

Portal vein thrombosis

Portal venous thrombosis may also occur during pregnancy, even in the absence of Budd–Chiari syndrome. This is a rarer phenomenon than Budd–Chiari syndrome in pregnancy, and patients with local abdominal risk factors such as cirrhosis, intra-abdominal infections, or malignancies are at higher risk than pregnant women for this condition [27]. Clinically, portal vein thrombosis may present with abdominal pain, nausea, vomiting, fever, and ascites, though some patients are asymptomatic. Presentation is considered acute if symptoms occur within 60 days of a confirmed diagnosis of portal vein thrombus [37]. Imaging findings at ultrasound are of heterogeneous



Fig. 8 A 46-year-old woman with new onset ascites and abnormal liver function tests. Coronal contrast-enhanced CT shows non-occlusive portal vein thrombus (arrow), splenomegaly, and ascites

thrombus within the portal vein, which is usually expanded in caliber. At color and spectral Doppler interrogation, flow may be absent, diminished, or reversed. Collateral vessels of cavernous transformation may begin to form within weeks of incident thrombosis. With CT, acute portal venous thrombus appears hyperdense on non-contrast examination, and the portal vein does not enhance as expected following contrast administration (Fig. 8). Of note, mural enhancement of the vein reflecting inflammation and/or peripheral intraluminal enhancement about non-occlusive thrombus may be noted [37]. On MRI, acute portal vein thrombus may appear heterogeneous and hyperintense on both T1-weighted and T2-weighted sequences, particularly in the acute setting [37].

Reproductive

Both benign and malignant processes may be identified within the reproductive organs, specifically, the uterus and ovaries, in response to changes in estrogen. Additionally, tamoxifen, a selective estrogen-receptor modulator (SERM) used in the treatment of hormone receptor-positive breast cancer, also has a stimulating effect specifically on the endometrium akin to endogenous estrogen, which can also lead to specific imaging findings [2, 38].

Endometrium

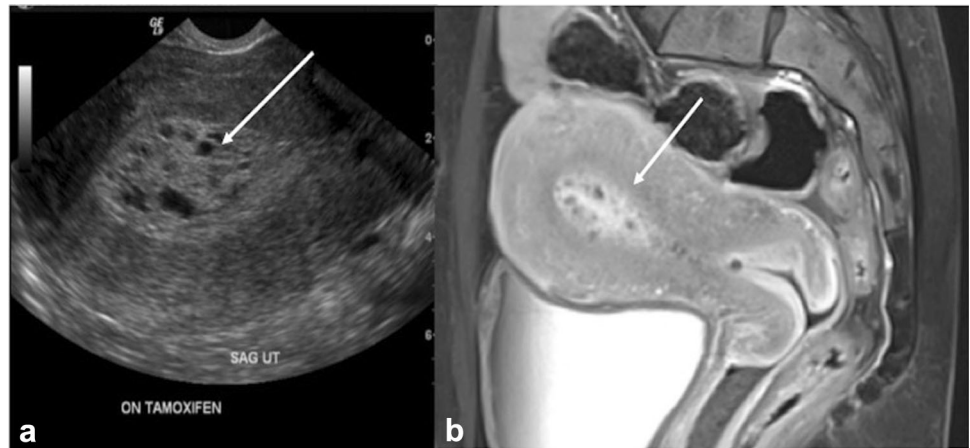
As a target organ of estrogen, the endometrium is exquisitely sensitive to increased exposure. Unopposed activation of estrogen receptors, which may be caused by elevated estrogen in the setting of obesity, anovulation, estrogen-secreting tumors, hormone replacement therapy, or the SERM tamoxifen, is the most common cause of endometrial hyperplasia and carcinoma [38, 39]. Pathologic changes of the endometrium span a spectrum from hyperplasia, to hyperplasia with atypia, to carcinoma. The most common presenting symptom of endometrial hyperplasia and carcinoma is abnormal vaginal bleeding, either in post-menopausal women or irregular cycles and spotting in pre-menopausal women. Abnormal vaginal bleeding is one of the most common reasons for gynecologic referral to radiologic evaluation [38, 40].

Endometrial hyperplasia and carcinoma

Ultrasound is usually the appropriate initial imaging modality for evaluation of suspected gynecologic pathology. MR imaging is a useful adjunct for additional characterization, diagnostic confirmation, and staging disease, as appropriate [39, 41]. In pre-menopausal women, the endometrium increases in thickness physiologically during

Fig. 9 A 50-year-old woman with history of DCIS, taking Tamoxifen, who presented with vaginal bleeding.

a Transvaginal ultrasound in longitudinal plane shows thickened, heterogeneous, endometrium with irregular cystic spaces. **b** Sagittal contrast-enhanced MRI also shows thickened endometrium with numerous non-enhancing cystic spaces. Pathology from endometrial biopsy revealed endometrial hyperplasia with atypia



the proliferative phase of the menstrual cycle and generally does not exceed 15 mm, although no definitive values are established in the literature. A 5 mm thickness cutoff is generally used for recommending endometrial sampling in post-menopausal women with bleeding [39]. Normal endometrial thickness for post-menopausal women without bleeding has not been as definitively established, and has been described as thick as 11 mm [39].

Endometrium is best evaluated at ultrasound utilizing an endovaginal approach. The endometrium should be visualized in its entirety to ensure the thickest area is measured and reported [38, 39]. Hyperplastic endometrium may undergo cystic changes with irregular margins with or without increased vascularity. These cystic changes are frequently seen in the setting of tamoxifen exposure (Fig. 9). Unlike other SERMs, tamoxifen exerts a stimulatory pro-estrogenic effect on the endometrium [42]. It is important to evaluate the endometrium carefully for invasive components if any of these findings are present. With MRI, the endometrium is T1 isointense to hypointense, T2 hyperintense, and should enhance homogeneously upon contrast administration. Cystic changes are best appreciated as non-enhancing regions on post-contrast sequences (Fig. 9) [41]. The CT appearance of endometrial hyperplasia is non-specific, as the endometrium is difficult to differentiate and/or measure separately from the adjacent myometrium. Regardless of imaging modality, differentiation between endometrial hyperplasia and endometrial cancer based on imaging alone is impossible and tissue sampling must be pursued when abnormal endometrium is seen on imaging.

Endometrial carcinoma is the most common gynecologic malignancy in industrialized nations, and is the cancer most closely linked to obesity in women [4]. Extra-ovarian estrogen production via adipose tissue is thought to be responsible for the hyperestrogenemic state in obese patients. There are two histologic subtypes of endometrial

carcinoma. Most commonly encountered is the type 1 (endometrioid) cancer, accounting for up to 90% endometrial carcinoma, which is more closely associated with obesity [4]. Type 2 includes the more aggressive serous papillary and clear cell adenocarcinoma subtypes, which are phenotypically closer to ovarian neoplasms and have a higher incidence of lymph node and distant metastases at diagnosis. These subtypes are indistinguishable at imaging. Treatment includes surgery, chemotherapy, and/or radiation depending on stage of disease [41]. At ultrasound, endometrial carcinoma appears as heterogeneous endometrial thickening or a focal polypoid mass (Fig. 10). Doppler imaging may demonstrate hypervascularity. A feeding vessel (vascular stalk) may be present in polypoid lesions; however, polyps can be either benign or malignant, and the presence of vascularity should not be interpreted as evidence for malignancy, nor should the absence of vascularity be interpreted as confirmation of benignity [38, 39]. At CT, heterogeneous endometrial thickening and/or enhancement may be seen (Fig. 10). MRI enables more detailed assessment of myometrial invasion [41, 43]. Usually, endometrial carcinoma is T1 isointense, T2 hypointense relative to the normal T2 hyperintense endometrium, and on post-contrast images demonstrate hypoenhancement relative to enhancing endometrium and myometrium. Diffusion-weighted imaging (DWI) and apparent diffusion coefficient (ADC) maps may be useful in identifying unanticipated metastases, including any cervical or vaginal drop metastases or suspicious lymph nodes [41].

Vagina/cervix

Clear cell adenocarcinoma (CCA) is a rare neoplasm of the cervix and vagina; the major risk factor for its development is in utero exposure to maternally ingested diethylstilbestrol (DES) [44]. This medication was prescribed with the

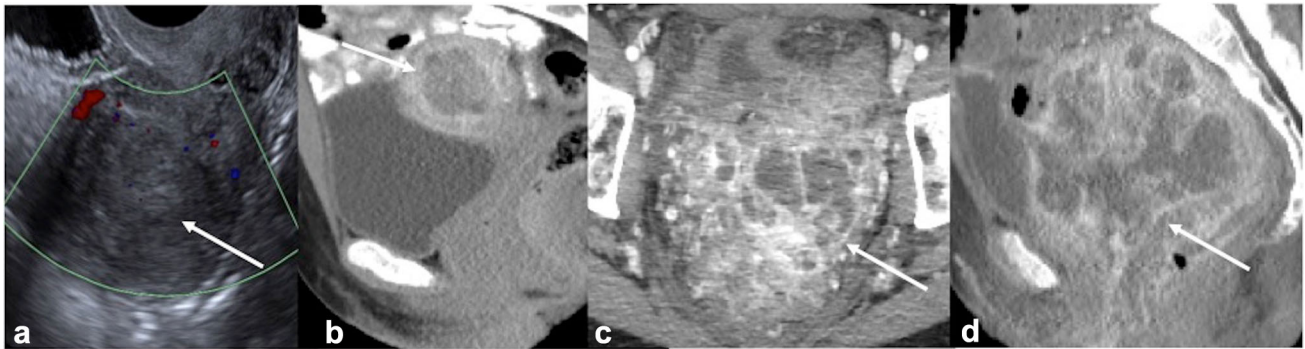


Fig. 10 A 62-year-old woman with history of > 5 years of hormone replacement therapy who presented with post-menopausal bleeding. **a** Transvaginal ultrasound shows large heterogeneous endometrial mass. Endometrial biopsy confirmed high-grade endometrioid adenocarcinoma. **b** Initial staging CT showed thickened, enhancing endometrium without definite intra-abdominal metastatic disease. Hysterectomy and bilateral salpingo-oophorectomy was performed

following this staging CT. **c** Axial and **d** sagittal reformat of CT performed for pelvic pain at four weeks of post-surgery shows a complex solid and cystic pelvic mass. Differential considerations included post-operative collection (hematoma versus abscess) and recurrent/residual disease. Surgical biopsy confirmed residual disease with possible transformation to sarcomatous features and/or dedifferentiation

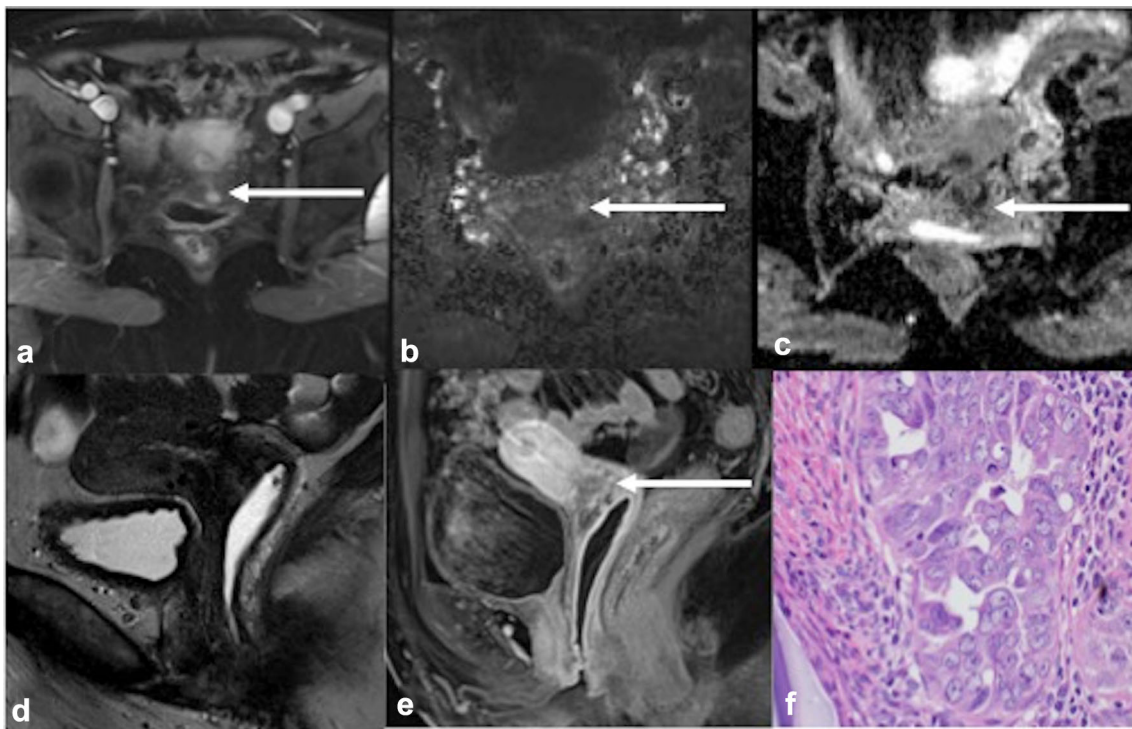


Fig. 11 A 67-year-old woman with history of in utero diethylstilbestrol (DES) exposure and with recent Pap smear positive for adenocarcinoma. **a** Axial arterial phase MRI pelvis shows an enhancing cervical mass. **b** Diffusion-weighted sequence and

c ADC map confirm restricted diffusion. **d** Sagittal T2-weighted and **e** sagittal post-contrast T1-weighted images better demonstrate the extent of the heterogeneous cervical mass. **f** Surgical pathology at time of hysterectomy confirmed clear cell adenocarcinoma

highest frequency in the early 1950s for preterm labor, as such, the cohort with highest risk was born between 1951 and 1956. However, the medication was reportedly given to patients until 1969, so the number of at-risk women may be larger than initially suspected. Rarely, clear cell adenocarcinoma of the cervix may arise in post-menopausal women without a history of DES exposure. Patients present

with abnormal vaginal bleeding, similar to presentations of other types of cervical and vaginal malignancies. With ultrasound, CCA of the cervix and/or vagina confers a spectrum of imaging findings, from focal or circumferential vaginal mural thickening to a multicystic mass which may protrude from the vaginal vault. With CT, solid components of a mass may enhance, while cystic components do

not [48]. With MRI, CCA appears as a polypoid or sessile vaginal or cervical mass with variable (hyperintense, intermediate, or hypointense) T2 signal, that often restricts diffusion (Fig. 11) [46]. CCA of the cervix or vagina is characteristically isointense to the vaginal wall on T1-weighted non-contrast images, with post-contrast enhancement usually seen [45].

Ovaries

Polycystic ovarian syndrome

Polycystic ovarian syndrome (PCOS) is the most common endocrine abnormality of pre-menopausal women [47]. PCOS is characterized by increased circulating androgens secondary to abnormal function of the hypothalamic-pituitary-gonadal axis. The direct etiology of PCOS is unknown, but is thought to relate to insulin resistance. Due to the abnormal pituitary function, increased levels of luteinizing hormone (LH) are present. The increased ratio of luteinizing hormone to follicle-stimulating hormone causes the ovaries to preferentially produce androgens. The increased androgen presence is thought to disrupt ovulation by disrupting follicular maturation, causing ovarian dysfunction and anovulation/oligo-ovulation [47, 48].

Diagnostic criteria for PCOS vary by expert group, but most diagnostic schema include some combinations of hyperandrogenism (clinical and/or biochemical), ovarian dysfunction, polycystic ovary morphology (PCOM), and other diagnoses excluded [47, 48]. At ultrasound or MRI, a polycystic ovary contains multiple similar-sized small cysts about the periphery of the ovary without a dominant follicle, due to the arrested follicular development in the setting of increased androgen exposure (Fig. 12) [47]. T2

hypointense central ovarian stroma with the “string of pearls” of peripheral cysts is the MRI imaging hallmark. CT is not as useful in assessment of the presence or number of ovarian follicles. With ultrasound, follicle number per ovary (FNPO) can be assessed and described. The threshold FNPO for diagnosis of PCOM has increased alongside improvements in ultrasound technology; while this number used to be 12, the number of follicles present to constitute polycystic morphology is now considered to be > 26 using a > 8 MHz transducer. [49]. The previously described criteria of ovarian volume of over 10 mL have not changed, though the volume measurement should not include corpora lutea, cysts, nor dominant follicles [50]. Of note, PCOM identified at ultrasound without relevant clinical history is not sufficient to confirm the diagnosis of PCOS, especially in adolescents [51].

Theca lutein cysts

Theca lutein cysts describe multiple ovarian cysts and large follicles that arise in the setting of exposure to high levels of beta-human chorionic gonadotropin (HCG). The most common causes of high levels of beta-HCG include multiple gestations and gestational trophoblastic disease; however, rarer etiologies include secretion by neoplasms [52].

Theca lutein cysts are usually evaluated with ultrasound as they most commonly occur in pregnant women. Sonographic appearance is that of multiple anechoic cysts and large follicles in an enlarged ovary (Fig. 13). At MRI, theca lutein cysts will have variable T1 and T2 signal intensity due to varying degrees of intracystic hemorrhagic contents. Theca lutein cysts may resolve as a normal gestation progresses. Typically, patients are asymptomatic,

Fig. 12 A 32-year-old woman undergoing evaluation for infertility. **a, b** Transvaginal ultrasound shows enlarged left ovary with multiple similar small peripherally situated follicles, which number greater than 26 at additional views. Ovarian volume measured > 10 mL. This ovary meets criteria to be described as polycystic

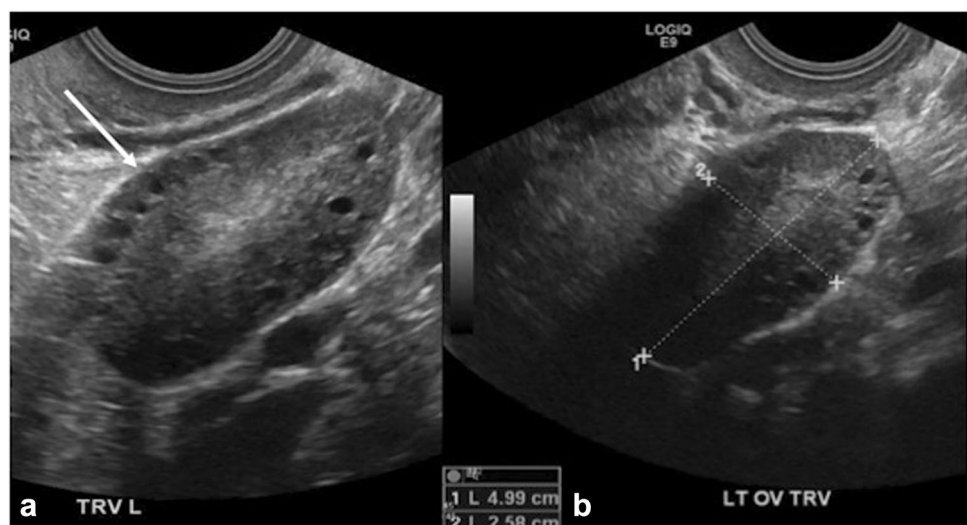


Fig. 13 **a** Transabdominal ultrasound of a pregnant patient at 14 weeks of gestation shows enlarged left ovary with multiple anechoic cysts. **b** Follow-up at 30 weeks of gestation shows resolution of the cysts with normal size and appearance of the left ovary. **c** Coronal contrast-enhanced CT of a different patient with complete hydatidiform molar pregnancy shows enlarged bilateral ovaries with multiple enlarged cysts

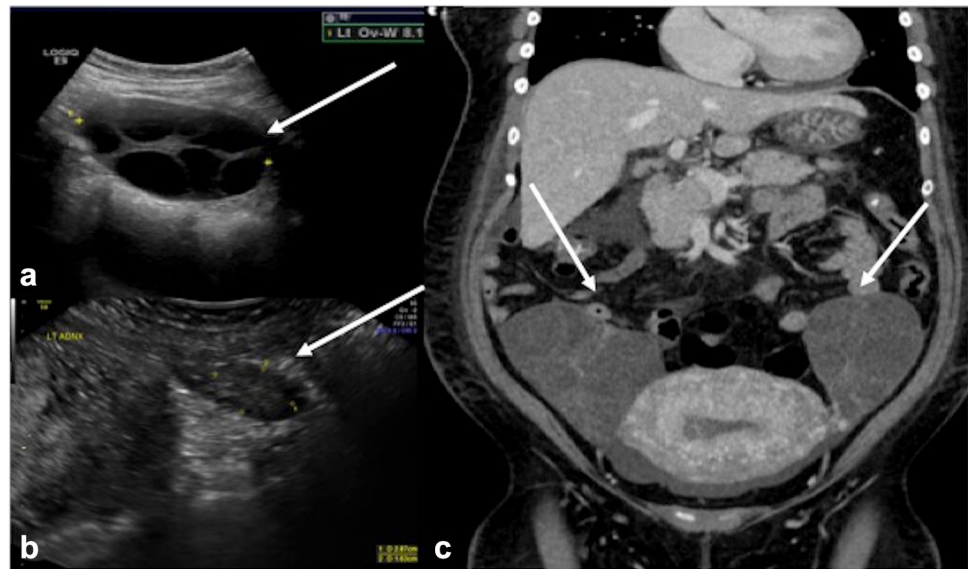


Fig. 14 A 28-year-old woman with positive pregnancy test and vaginal bleeding. **a** Transvaginal ultrasound of a patient with elevated b-HCG shows markedly thickened endometrium with multiple cystic

spaces. **b** Axial contrast-enhanced CT and **c** axial T1-weighted contrast-enhanced MRI show robust enhancement of solid components. Final pathology confirmed choriocarcinoma

though may report pelvic pain in the setting of cyst hemorrhage or rupture [52].

Gestational trophoblastic disease (GTD), a major risk factor for theca lutein cyst development, includes both molar pregnancy and gestational trophoblastic neoplasia. Theca lutein cysts are seen in up to 20% cases of complete hydatidiform molar pregnancy [53]. Hydatidiform molar pregnancies (both complete and partial) occur in approximately 1 in 1,500 pregnancies in the United States and up to 2 in 1,000 pregnancies in Southeast Asia [53]. This process arises from aberrant chromosomal duplication and trophoblastic proliferation resulting in abnormal growth of placental villi [53, 54]. Imaging of gestational trophoblastic disease usually occurs first with ultrasound, given that pregnancy is suspected. Ultrasound shows abnormally thickened endometrium with multiple cystic spaces (Fig. 14). Fetal parts may be seen in the setting of partial mole. Imaging findings must be interpreted in context with

HCG levels, as the diagnosis cannot be made with imaging alone, given that sonographic mimics of GTD include processes such as reactive decidual changes (including that of normal early pregnancy), hydropic endometrial degeneration, and retained products of conception.

The spectrum of gestational trophoblastic neoplasia (GTN) includes both invasive mole and choriocarcinoma, as well as rarer entities such as placental site trophoblastic tumor and epithelioid trophoblastic tumor [54]. GTN may occur following a molar pregnancy (25% of cases) but more commonly occurs following pregnancy ended at term (50% cases) or earlier (25% cases) [53, 54]. Choriocarcinoma occurs in 1 in 20,000–40,000 pregnancies, and metastases are present in up to 30% patients at time of diagnosis [54]. Imaging features of invasive mole and choriocarcinoma are similar, generally, of a non-specific heterogeneous uterine mass invading into or through the myometrium, and final diagnosis is made at histology

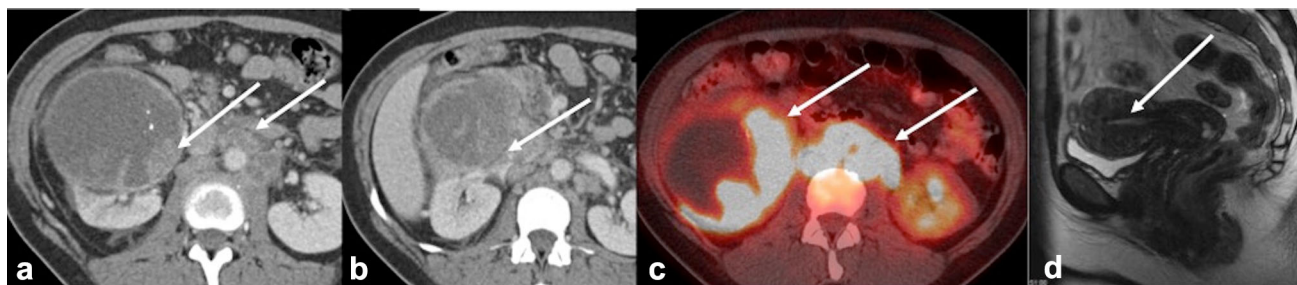


Fig. 15 A 44-year-old woman with right flank pain and elevated HCG who was referred for imaging based on clinical concern for gestational trophoblastic disease. **a** Axial contrast-enhanced CT shows a large heterogeneous right renal mass, large retroperitoneal lymphadenopathy, and **b** involvement of the IVC. **c** Fused axial images from FDG-PET/CT show marked FDG-avidity of the tumor

(Fig. 14). MRI is superior to US for evaluation of both extent of pelvic invasion and for assessment of lymphadenopathy [55].

Rarely, non-gynecologic malignancies, including breast, lung, gastric, colon, and pancreaticobiliary tumors may also produce HCG, typically in more aggressive lesions [56]. Elevated levels of HCG have been reported in up to 23% cases of renal cell carcinoma [59]. Serum HCG levels in the setting of renal cell carcinoma are a prognostic factor independent of grade and stage and usually portend poor prognosis [57]. Chromophobe type renal cell carcinoma is the most common histologic variant associated with a high level of HCG [58]. Sarcomatoid renal cell carcinoma is a rare subtype which has been reported to arise associated with chromophobe cell carcinomas; this variant portends the worst prognosis of all renal cell carcinoma (Fig. 15) [57, 58]. Finally, given the similar subunit structure of HCG and thyroid stimulating hormone (TSH), theca lutein cysts have been reported to develop in rare cases of severe hypothyroidism [59].

and the lymphadenopathy. **d** Sagittal T2-weighted image from MRI pelvis also performed for workup of elevated HCG demonstrates uterine fibroids with normal endometrium, with no evidence to suggest gestational trophoblastic disease. Pathology confirmed sarcomatoid carcinoma arising from chromophobe renal cell carcinoma, the subtype of RCC most likely to express high levels of HCG

Ovarian hyperstimulation syndrome

Ovarian hyperstimulation syndrome (OHSS) describes the constellation of signs and symptoms of cystic enlargement of the ovaries and extravascular fluid shifts in the setting of exogenous administration of LH and/or beta-HCG for assisted reproductive technology (ART) [52]. Hyperstimulated ovaries produce vascular-endothelial growth factor (VEGF), which causes increased vascular permeability and is thought to be the etiology of the extravascular fluid shifts associated with OHSS. Patients with OHSS usually present with nausea/vomiting in the setting of ART. Complications include adnexal torsion of massively enlarged ovaries, ascites, pleural effusions, pulmonary edema, and hypercoagulability. Several classifications schemes exist to assign severity; these largely rely on clinical factors [52].

Imaging findings at ultrasound include enlarged ovaries with multiple follicles and corpus luteal cysts, which may be anechoic or hemorrhagic, described with a “spoke-wheel” pattern on US as well as CT and MR (Fig. 16) [60]. Differentiation from torsion is important, as such, the location of follicles can be helpful. In the clinical scenario of torsion, follicles are usually peripheralized due to

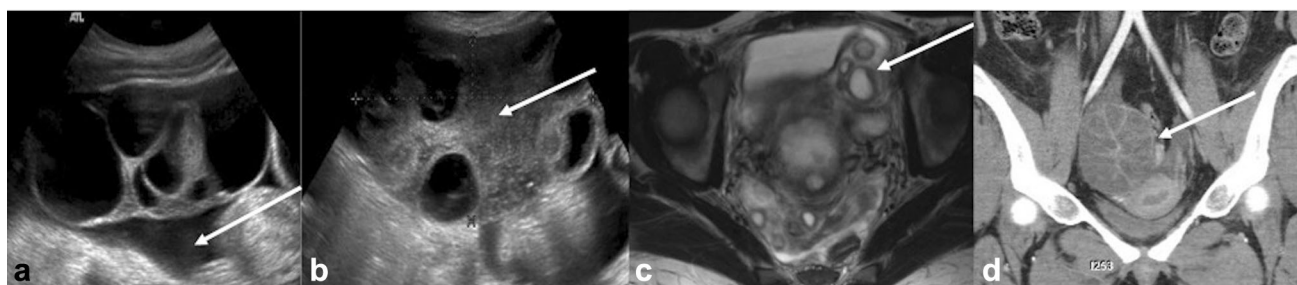


Fig. 16 A 36-year-old woman undergoing fertility treatment who presents with abdominal pain and distention. **a** Transvaginal ultrasound image of the right ovary demonstrates marked enlargement with multiple cysts. Free pelvic fluid is also present. **b** Transvaginal ultrasound image of the left ovary demonstrates similar enlargement

with prominent edematous stroma. **c** Axial T2-weighted MRI pelvis demonstrates multiple follicles/luteinized cysts in each ovary. **d** Coronal CT demonstrates the enlarged peripheral follicles appearing in a classic “spoke-wheel” pattern

stromal edema. OHSS is usually not accompanied by stromal edema, and follicles are more uniformly distributed in these enlarged ovaries [52]. Large volume ascites and pleural effusions may be seen. Not all pelvic fluid in ART patients is ascites related to OHSS; however, in the appropriate clinical setting, the presence of pelvic free fluid may prompt suspicion or further evaluation for ruptured ectopic/heterotopic pregnancy.

Endometrioma

Endometriosis is characterized by the presence of ectopic endometrium outside the endometrial cavity, most commonly in the ovaries. Other common locations include the pelvic cul-de-sac, mesentery, and uterosacral ligaments [61]. Endometrioma describes this ectopic tissue implanted on the ovary, and is generally described as a cystic adnexal lesion containing variable amounts of blood products. The endometrium in these ectopic sites remains responsive to both endogenous estrogen as well as SERMs, and consequently a woman with continued hormone exposure may report continued symptoms related to the ectopic tissue [61].

At ultrasound, an endometrioma may appear as a cyst with diffuse homogeneous low-level echoes (Fig. 17). Differential considerations would include a hemorrhagic ovarian cyst if the lesion has not been seen at prior imaging. If present, punctate echogenic foci within the cyst wall help confirm the diagnosis of endometrioma. These are believed to be hemosiderotic nodules in the wall of these cysts [61]. At MRI, an endometrioma is intrinsically T1 hyperintense owing to the presence of blood products. At T2-weighted imaging, endometriomas demonstrated varying degrees of “shading” denoting layering hemorrhagic and/or proteinaceous products (Fig. 17) [62]. A “T2 dark spot” sign of a discrete hypointense focus adjacent to, but not within, the cyst wall has also been described, related to chronic and repeated hemorrhage, which can help

differentiate from a hemorrhagic cyst [63]. A cyst-within-cyst appearance may be seen, indicating multiple prior episodes of intracystic hemorrhage [61]. Surgical removal is generally recommended for endometriomas due to a risk of malignant transformation, usually to an endometrioid or clear cell type carcinoma [64]. If not removed, annual surveillance ultrasound is recommended to assess for any worrisome features, specifically, any development of vascularity associated with mural nodules would raise suspicion for the presence of neoplasm [61, 64, 65].

Sex cord-stromal tumors

Sex cord-stromal tumors of the ovary describe tumors that arise from any of the sex cord or the stromal cell types that make up the organ. The sex cord cell types include granulosa cells and Sertoli cells, and the stromal cell types are theca cells, Leydig cells, and fibroblasts. Sex cord-stromal tumors account for approximately 8% of ovarian neoplasms. These tumors may be functional, secreting estrogen, inhibin, Mullerian-inhibiting substance, or androgens depending on the cell type. Granulosa cell tumors are the most common estrogen-secreting sex cord-stromal tumor and also the most common malignant sex cord-stromal tumor [37]. These lesions represent approximately 5% of ovarian neoplasms and occur in a bimodal age distribution, affecting women both early (pre-puberty) and later (post-menopausal) in life. Pre-pubertal girls are affected by juvenile granulosa cell tumors, which may cause precocious puberty due to their functional secretion of estrogen. It has been reported that up to 10% precocious puberty in girls is due to juvenile granulosa cell tumors [66]. Post-menopausal women with granulosa cell tumor may present with abnormal bleeding, and additionally are at increased risk for endometrial carcinoma, which has been reported in up to 25% cases of adult granulosa cell tumor [67]. Prognosis is generally good, with > 90% 10-year survival, though recurrence is possible even 10–20 years following

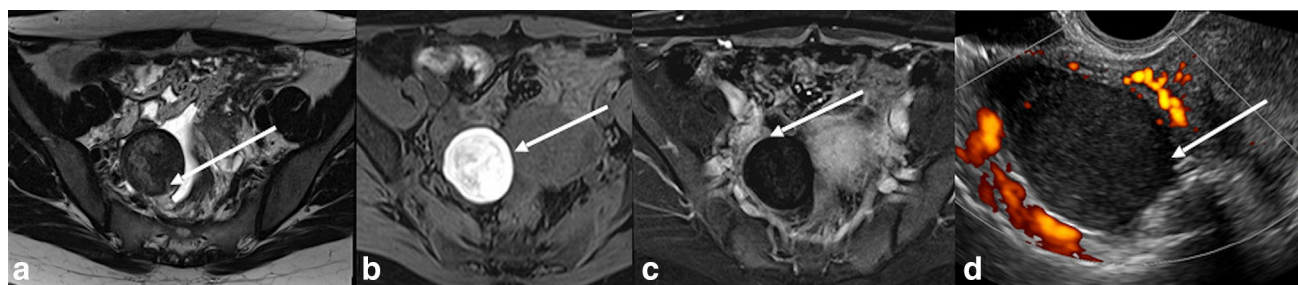


Fig. 17 A 55-year-old woman with history of DCIS, taking Tamoxifen. **a** Axial T2 MR image shows right ovarian lesion that is T2 hypointense with a “dark spot” (arrow). **b** Axial T1 fat-suppressed pre-contrast MR image shows the intrinsic T1 hyperintense signal of the lesion. **c** Axial T1 fat-suppressed post-contrast subtraction MR

image shows thin peripheral enhancement (arrow). **d** Ultrasound of the lesion shows an adnexal cyst with diffuse low-level echoes and peripheral vascularity. The constellation of findings is compatible with endometrioma

Fig. 18 A 68-year-old woman with pelvic pain and distention. **a** Axial contrast-enhanced CT and **b** transvaginal ultrasound show large, heterogeneous, multiseptated pelvic mass. Ultrasound better demonstrates varying intracystic echogenicity suggesting differing degrees of intracystic hemorrhage. Pathology confirmed granulosa cell tumor at surgical resection

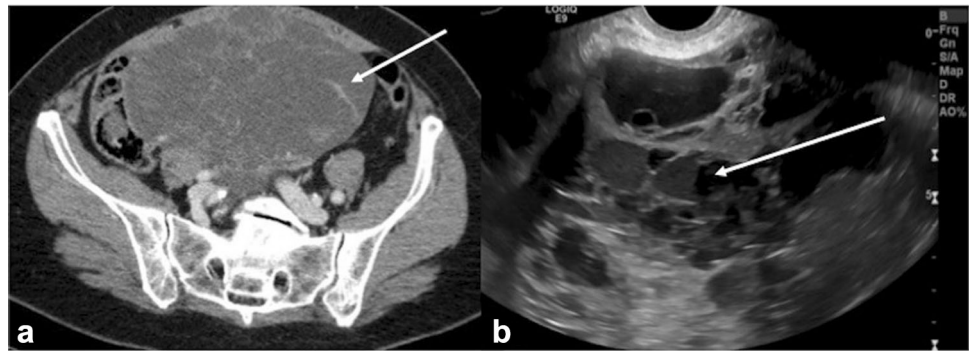
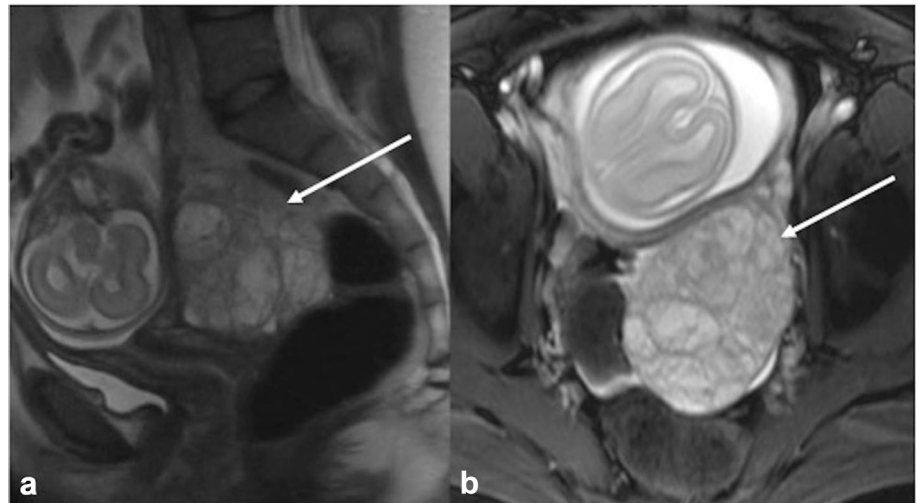


Fig. 19 A 24-year-old woman, G2P1, at 23 weeks of gestation, with left adnexal mass incidentally discovered at first trimester ultrasound. **a** Sagittal T2 HASTE and **b** axial truFISP images demonstrate multicystic heterogeneous left ovarian mass and a gravid uterus. Pathology confirmed mixed tumor, 90% juvenile granulosa cell tumor, and 10% gonadoblastoma/dysgerminoma



diagnosis and treatment [67]. At imaging, granulosa cell tumors are solid or multicystic ovarian masses with varying degrees of intracystic hemorrhage and central fibrosis [67]. The solid and hemorrhagic components demonstrate varying degrees of increased echogenicity at ultrasound (Fig. 18), and varying signal T1 and T2 signal intensities at MRI, depending on the age of hemorrhage (Fig. 19) [67]. Ascites may accompany the first presentation of these masses. The CT appearance is non-specific, and may show differing densities of the different cystic, solid, and hemorrhagic components (Fig. 18).

Sertoli–Leydig cell tumors represent the most common type of androgen-secreting sex cord-stromal ovarian tumor, though only make up 0.5% ovarian neoplasms [68]. Sertoli cells are found in the normal testis and are responsible for testicular tubular formation; they are not present in the normal ovary. Most Sertoli–Leydig cell tumors arise in women under the age of 30, and approximately 30% of these patients develop virilization related to the increased androgen exposure. Very rarely, Sertoli–Leydig cells have been reported to secrete other substances, including alpha-fetoprotein [68]. At imaging, a Sertoli–Leydig cell tumor appears as a solid or multicystic mass, generally hypoechoic at ultrasound and demonstrating post-contrast

enhancement at pelvic CT or MRI. In symptomatic patients, the tumor may be very small and difficult to appreciate at imaging. In these patients, ovarian vein sampling may be warranted [68].

Krukenberg metastases

Ovarian metastases of gastrointestinal tract tumors, also known as Krukenberg tumors, may also exhibit functional endocrine behavior [69]. Both hyperestrogenic as well as androgenic activity and symptoms of virilization have been reported both in pregnant and non-pregnant women with Krukenberg tumors, related to the proliferation of ovarian stroma in the setting of lesion growth [69, 70]. Early identification and treatment may limit the endocrine activity and therefore reduce patient symptoms [69].

Musculoskeletal

Several hormones act to alter osseous structures, primarily through effects on cells responsible for bone creation and resorption, osteoblasts and osteoclasts. Estrogen is also active in the bones, by blocking synthesis of interleukin-6,

a stimulator of bone resorption, and inducing apoptosis of osteoclasts [71]. Decreased circulating active estrogen, for example with menopause, or inactivation of specific estrogen receptors via SERMs, allows for unopposed bone resorption and proliferation of osteoclasts and may be visible as osteopenia on abdominal imaging.

Conclusions/summary

Hormonal abnormalities are systemic disorders in which the imaging findings may occur distant from the causative sites, particularly in the setting of abnormalities of estrogen exposure. Multiple imaging findings that are either the result of or even the etiology of hyperestrogenemia may be seen in the abdomen and pelvis. Understanding the biochemical and hormonal changes behind these findings can assist radiologists in suggesting the root cause of clinical symptoms. Recognition of these findings and knowledge of associated conditions will enable the radiologist to make meaningful contributions to the care of these patients.

References

- Conn P.M (2005). Introduction to Endocrinology. In: Melmed S., Conn P.M. (eds) Endocrinology. Humana Press: Totowa.
- Hata S, Miki Y, Saito R, et al. (2013) Aromatase in human liver and its diseases. *Cancer Medicine* 2:305-315.
- Yager JD, Davidson NE. (2006) Estrogen carcinogenesis in breast cancer. *N Engl J Med*; 354:270-282.
- Onstad MA, Schmandt RE, Lu KH. (2016) Addressing the role of obesity in endometrial cancer risk, prevention, and treatment. *J Clin Oncol*; 34: 4225-4230
- Harada N, Ota H, Yoshimura N, Katsuyama T, Takagi Y. (1998) Localized aberrant expression of cytochrome P450 aromatase in primary and metastatic malignant tumors of human liver. *J Clin Endocrinol Metab*; 83: 697-702.
- Wenniger LM, Terpstra V, Beuers U. (2010) Focal nodular hyperplasia and hepatic adenoma: epidemiology and pathology. *Dig Surg*; 27:24-31.
- Kaltenbach TE, Engler P, Kratzer W, et al. (2016) Prevalence of benign focal liver lesions: ultrasound investigation of 45,319 hospital patients. *Abdom Radiol*; 41:25-32.
- Karhunen PJ. (1986) Benign hepatic tumours and tumour like conditions in men. *J Clin Pathol*; 39:183-188.
- Venturi A, Piscaglia F, Vidili G, et al. (2007) Diagnosis and management of hepatic focal nodular hyperplasia. *J Ultrasound*; 10:116-127.
- Grazioli L, Abrosini R, Frittoli B, Grazioli M, Morone M. (2017) Primary benign liver lesions. *Eur J Radiol*; 95: 378-398.
- Fodor M, Primavesi F, Braunwarth E, et al. (2018) Indications for liver surgery in benign tumours. *Eur Surg*; 50: 125-131.
- Ringe KI, Husarik DB, Sirlin CB, Merkle EM. (2010) Gadoteric acid-enhanced MRI of the liver: part I, protocol optimization and lesion appearance in the noncirrhotic liver. *Am J Roentgenol*; 195:13-28.
- Grazioli L, Bondioni MP, Haradome H, et al. (2012) Hepatocellular adenoma and focal nodular hyperplasia: value of gadoteric acid-enhanced MR imaging in differential diagnosis. *Radiology*; 262: 520-529.
- Casarella WJ, Knowles DM, Wolff M, Johnson PM. (1976) Focal nodular hyperplasia and liver cell adenoma: radiologic and pathologic differentiation. *Am J Roentgenol*; 131:393-402.
- Venkatesh K. (2014) Liver masses: a clinical, radiological, and pathological perspective for: Perspectives in clinical gastroenterology and hepatology. *Clin Gastroenterol Hepatol*; 12: 1414-1429.
- Virgilio E, Cavallini M. (2018) Managing focal nodular hyperplasia of the liver: surgery or minimally invasive approaches? A review of the preferable treatment options. *Anticancer Res*; 38: 33-36.
- Kuo YH, Wang JH, Lu SN, et al. (2009) Natural course of hepatic focal nodular hyperplasia: a long-term follow-up study with sonography. *J Clin Ultrasound*; 37: 132-137.
- Agrawal S, Agarwal S, Arnason T, et al. (2015) Management of hepatocellular adenoma: recent advances. *Clin Gastroenterol Hepatol*; 7:1221-1230
- Stoot J, Coelen R, de Jong MC, Dejong C. (2010) Malignant transformation of hepatocellular adenomas into hepatocellular carcinomas: a systematic review including more than 1600 adenoma cases. *HPB (Oxford)*; 12:509-522.
- Grazioli L, Federle M, Brancatelli G, et al. (2001) Hepatic adenomas: imaging and pathologic findings. *Radiographics*; 21: 877-894.
- Van Aalten SM, Thomeer MGJ, Terkivatan T, et al. (2011) Hepatocellular adenomas: correlation of MR imaging findings with pathologic subtype classifications. *Radiology*; 261:172-181.
- Reizine E, Amaddeo G, Pigneur F, et al. (2018) Quantitative correlation between uptake of Gd-BOPTA on hepatobiliary phase and tumor molecular features in patients with benign hepatocellular lesions. *Eur Radiol*. <https://doi.org/10.1007/s00330-018-5438-7>
- Guo Y, Li W, Xie Z, et al. (2017) Diagnostic value of Gd-EOB-DTPA-MRI for hepatocellular adenoma: a meta-analysis. *J Cancer*; 8:1301-1310.
- Agarwal S, Fuentes-Orrego JM, Amason T, et al. (2014) Inflammatory hepatocellular adenomas can mimic focal nodular hyperplasia on gadoteric acid-enhanced MRI. *Am J Roentgenol*; 203: W408-414.
- Cobey FC, Salem RR. (2004) A review of liver masses in pregnancy and a proposed algorithm for their diagnosis and management. *Am J Surg*; 187: 181-191.
- Thomeer MG, Broker M, Verheij J, et al. (2016) Hepatocellular adenoma: when and how to treat? Update of current evidence. *Therap Adv Gastroenterol*; 9: 898-912.
- Almashhrawi AA, Ahmed KT, Rahman RN, Hammoud GM, Ibdah JA. (2013) Liver diseases in pregnancy: diseases not unique to pregnancy. *World J Gastroenterol*; 19: 7630-7638.
- Bonnar J. (1987) Coagulation effects of oral contraception *Am J Obstet Gynecol*; 157:1042-1048.
- Bissonnette J, Durand F, de Raucourt E, et al. (2015) Pregnancy and vascular liver disease. *J Clin Exp Hepatol*; 5:41-50.
- Shin N, Kim YH, Xu H, et al. (2016) Redefining Budd-Chiari syndrome: a systematic review. *World J Hepatol*; 8: 691-702.
- Dilawari J.B., Bamberg P., Chawla Y. (1994) Hepatic outflow obstruction (Budd-Chiari syndrome). Experience with 177 patients and a review of the literature. *Medicine (Baltimore)*;73:21-36.
- Brancatelli G, Vilgrain V, Federle MP, et al. (2007) Budd-Chiari syndrome: spectrum of imaging findings. *Am J Roentgenol*; 188: W168-W176.
- Ferra H, Behrens G, Lopera J. (2012) Budd-Chiari syndrome. *Am J Roentgenol*; 199: 737-745.

34. Vilgrain V, Lewin M, Vons C, et al. (1999) Hepatic nodules in Budd-Chiari syndrome: imaging features. *Radiology*; 210:443–450
35. Brancatelli G, Federle MP, Grazioli L, Golfieri R, Lencioni R. (2002) Large regenerative nodules in Budd-Chiari syndrome and other vascular disorders of the liver: CT and MR imaging findings with clinico-pathologic correlation. *Am J Roentgenol*; 178:877–883.
36. Ruh J, Malago M, Busch Y, et al. (2005) Management of Budd-Chiari syndrome. *Dig Dis Sci*; 50:540–546
37. Jha RC, Khera SS, Kalaria AD. (2018) Portal vein thrombosis: imaging the spectrum of diseases with an emphasis on MRI features. *Am J Roentgenol*; 211:14–24.
38. Davidson KG, Dubinsky TJ. (2003) Ultrasonographic evaluation of the endometrium in postmenopausal vaginal bleeding. *Radiol Clin N Am*; 41:769–780.
39. Smith-Bindman R, Kerlikowske K, Feldstein VA, et al. (1998) Endovaginal ultrasound to exclude endometrial cancer and other endometrial abnormalities. *JAMA*; 280:1510–1517.
40. Chandra V, Kim JJ, Benbrook DM, Dwivedi A, Rai R. (2016) Therapeutic options for management of endometrial hyperplasia. *J Gynecol Oncol*; 27:e8.
41. Freeman SJ, Aly AM, Kataoka MY, et al. (2012) The revised FIGO staging system for uterine malignancies: implications for MR imaging. *Radiographics*; 32:1805–1827.
42. Achiron R, Grisaru D, Golan-Porat N, Lipitz S. (1996) Tamoxifen and the uterus: an old drug tested by new modalities. *Ultrasound Obstet Gynecol*; 7:374–378.
43. Nougaret S, Horta M, Sala E, et al. (2018) Endometrial cancer MRI staging: updated guidelines of the European Society of Urogenital Radiology. *Eur Radiol*. <https://doi.org/10.1007/s00330-018-5515-y>
44. Huo D, Anderson D, Palmer JR, Herbst AL. (2017) Incidence rates and risks of diethylstilbestrol-related clear-cell adenocarcinoma of the vagina and cervix: update after 40-year follow up. *Gynecologic Oncology*; 146:566–571.
45. Gilles R, Michel G, Chancelier MD, Vanel D, Masselot J. (1993) Case report: clear cell adenocarcinoma of the vagina: MR features. *Br J Radiol*;66:168–70.
46. Parikh JH, Barton DPJ, Ind TEJ, Sohaib SA. (2008) MR imaging features of vaginal malignancies. *Radiographics*; 28:49–63.
47. Williams T, Mortada R, Porter S. (2016) Diagnosis and treatment of polycystic ovary syndrome. *Am Fam Phys*; 94:106–113.
48. Lee TT, Rausch ME. (2012) Polycystic ovarian syndrome: role of imaging in diagnosis. *Radiographics*; 32: 1643–1657.
49. Lujan ME, Chizen DR, Pierson RA. (2008) Diagnostic criteria for polycystic ovary syndrome: pitfalls and controversies. *J Obstet Gynaecol Can*; 30: 671–679.
50. Teede HJ, Misso ML, Costello MF, et al. (2018) International PCOS Network. Recommendations from the international evidence-based guideline for the assessment and management of polycystic ovary syndrome. *Clin Endocrinol*. <https://doi.org/10.1111/cen.13795>
51. Fitzgerald S, Divasta A, Gooding H. (2018) An update on PCOS in adolescents. *Curr Opin Pediatr*; 30:459–465.
52. Babagbemi KT, Arleo EK, Asrani AV, Troiano RN. (2013) Emergent complications of assisted reproduction: expecting the unexpected. *Radiographics*; 33:229–244.
53. Lurain JR. (2010) Gestational trophoblastic disease I: epidemiology, pathology, clinical presentation, and diagnosis of gestational trophoblastic disease, and management of hydatidiform mole. *Am J Obstet Gynecol*; 203: 531–539.
54. Lurain JR. (2011) Gestational trophoblastic disease II: classification and management of gestational trophoblastic neoplasia. *Am J Obstet Gynecol*; 204: 11–18.
55. Shaaban AM, Rezvani M, Haroun RR, et al. (2017) Gestational trophoblastic disease: clinical and imaging features. *Radiographics*; 37: 681–700.
56. Stenman UH, Alfthan H, Hotakainen K. (2004) Human chorionic gonadotropin in cancer. *Clin Biochem*; 37:549–561.
57. Hotakainen K. (2002) The free beta-subunit of human chorionic gonadotropin as a prognostic factor in renal cell carcinoma. *Br J Cancer*; 86:185–189.
58. Shimomura T. (2005) Sarcomatoid renal cell carcinoma with a chromophobe component producing beta-human chorionic gonadotropin. *Int J Urol*; 12: 835–837.
59. Rukundo J, Ntsumbumuyange D, Small M, Rulisa S, Bazzett-Matabele L. (2017) Theca lutein cysts in the setting of primary hypothyroidism. *Ultrasound in Obstetrics and Gynecology*; 50: EP25.13.
60. Jung BG, Kim H. (2001) Severe spontaneous ovarian hyperstimulation syndrome with MR findings. *J Comput Assist Tomogr*; 25: 215–217.
61. Woodward PJ, Sohaey R, Mezzetti TP. (2001) Endometriosis: radiologic-pathologic correlation. *Radiographics*; 21: 193–216.
62. Glastonbury CM. (2002) The shading sign. *Radiology*; 224:199–201.
63. Corwin MT, Gerscovich EO, Lamba R, Wilson M, McGahan JP. (2013) Differentiation of ovarian endometriomas from hemorrhagic cysts at MR imaging: utility of the T2 dark spot sign. *Radiology*; 271:126–132.
64. McDermott S, Oei TN, Iyer VR, Lee SI. (2012) MR imaging of malignancies arising in endometriomas and extra-ovarian endometriosis. *Radiographics*; 32:845–863.
65. Levine D, Brown DL, Andreotti RF, et al. (2010) Management of asymptomatic ovarian and other adnexal cysts imaged at US: Society of Radiologists in Ultrasound consensus conference statement. *Radiology*; 256:943–954.
66. Outware EK, Wagner BJ, Mannion C, et al. (1998) Sex cord-stromal and steroid cell tumors of the ovary. *Radiographics*; 18: 1523–1546.
67. Jung SE, Rha SE, Lee JM, et al. (2005) CT and MRI findings of sex cord-stromal tumor of the ovary. *Am J Roentgenol*; 185:207–215.
68. Horta M, Cunha TM, Marques RC, Felix A. (2014) Ovarian Sertoli-Leydig cell tumor with heterologous elements of gastrointestinal type associated with elevated serum alpha-fetoprotein level: an unusual case and literature review. *Radiology Case*; 8:30–41.
69. McGill FM, Ritter DB, Rickard CS, et al. (1999) Krukenberg tumors: can management be improved? *Gynecol Obstet Invest*; 48:61–65.
70. Bacchus H. (ed) (1975) Amenorrhea. In: *Essentials of Gynecologic and Obstetric Endocrinology*. Springer: Dordrecht. https://doi.org/10.1007/978-94-011-9834-9_6.
71. Syed FA, Oursler MJ, Hefferanm TE, et al. (2008) Effects of estrogen therapy on bone marrow adipocytes in postmenopausal osteoporotic women. *Osteoporos Int*; 19:1323–1330.